Multiple Time Constant Modeling of Dispersion Dynamics in Hetero Field-Effect Transistors

Ingmar Kallfass, Hermann Schumacher, *Member, IEEE*, and Thomas J. Brazil, *Fellow, IEEE*

***Abstract*—A new approach to the modeling of frequency dispersion effects encountered in the drain current characteristics of state-of-the-art hetero field-effect transistors is presented. The empirical, equivalent-circuit based model is dedicated to efficient microwave circuit design and allows for the inclusion of individual dispersion effects, taking into account their respective time constants. The proposed topology allows for small- and large-signal analysis in both the time and frequency domains. Parameter extraction and verification of the model is carried out using pulsed-*I–V* and dc measurements as well as microwave frequency *S*-parameter characterization of both a GaAs pseudomorphic high electron mobility transistor (pHEMT) and an InP pHEMT technology. Finally, the model is employed in the design and realization of a GaAs pHEMT traveling-wave monolithic microwave integrated circuit. Simulation results are compared to measurements with a focus on figures of merit which are affected by frequency dispersion.**

***Index Terms*—Integrated circuit modeling, MODFETs, semiconductor device modeling.**

I. Introduction

TODAY's high-performance hetero field-effect transistor (HFET) technologies show significant frequency-dispersive effects, mainly affecting the device's current–voltage (*IV*) characteristics by introducing a frequency and time dependence to drain current. Dispersion is observed in classical GaAs- and InP-based technologies as well as in the more recent GaN HFETs. Among the physical effects responsible for dispersion are thermal- or self-heating effects, predominantly in GaAs-based devices due to the substrate's low thermal conductivity. Trapping and detrapping of carriers and occupation of interface states are present in all HFET types and depend on layer and interface quality. Impact ionization, predominant in small bandgap devices like InGaAs/InP, but also occurring in other HFETs at high drain potentials, also introduces dispersive dynamic behavior. All of the above effects may empirically be described by their quantitative impact on device characteristics and an associated time constant or corner frequency.

Manuscript received October 12, 2005; revised February 13, 2006. The work of T. J. Brazil was supported by Science Foundation Ireland.

I. Kallfass was with the Department of Electron Devices and Circuits, University of Ulm, 89081 Ulm, Germany. He is now with the Fraunhofer Institute for Applied Solid-State Physics, 79108 Freiburg, Germany (e-mail: ingmar.kallfass@iaf.fraunhofer.de).

H. Schumacher is with the Department of Electron Devices and Circuits, University of Ulm, 89081 Ulm, Germany (e-mail: hermann.schumacher@uni-ulm.de).

T. J. Brazil is with the Department of Electronic and Electrical Engineering, University College Dublin, Dublin, Ireland (e-mail: tom.brazil@ucd.ie).

Digital Object Identifier 10.1109/TMTT.2006.875264

State-of-the-art modeling of frequency dispersion is generally focused on the physical description of one particular effect while neglecting the others. Since the impact of any of the above mentioned dispersion effects is most pronounced on output conductance, earlier dispersion models concentrated on the g_{ds} characteristics [1], [2]. Thermal models incorporate channel temperature as a variable of a thermal subcircuit [3]. An empirical circuit topology often encountered combines a static and a dynamic current source via a dc-blocking capacitor [4], [5]. Another empirical approach to modeling dispersion is the use of equivalent voltage sources in the FET circuit topology [6]. More recently, GaN-based devices have gained high importance due to their power capabilities at microwave frequencies. Frequency dispersion in these devices lead to the so-called radio-frequency (RF) current collapse [7]. Thermal and trap-related modeling of dispersion has been carried out, e.g., for GaN metal–semiconductor FET devices [8]. If at all, commercial models offer simple methods to include frequency dispersion, such as single time constant thermal subcircuits [9]. On the system level, frequency dispersion is responsible for memory effects and treated by behavioral modeling [10], [11].

Here, we describe an empirical, equivalent-circuit-based dispersion model dedicated to the efficient use in microwave circuit design. The new dispersion circuit topology offers accurate description of devices exhibiting different dispersion effects, taking into account their respective time constants and impact on *IV* characteristics. After introducing the modeling approach, the dispersion model is described in terms of small- and large-signal topologies and parameters. The model is then applied to a 0.15-μm AlGaAs/InGaAs/GaAs pHEMT technology [12] with a transit frequency of $f_T = 110$ GHz as well as to a 0.2-μm InP–InGaAs–InP pHEMT [13] with an f_T of 120 GHz. Although not discussed in this paper, the same dispersion modeling technique has been found to be applicable to a Si-based technology, namely, a 0.1—μm strained-Si/SiGe MODFET [14]. The model is verified and shown to accurately predict dispersion dynamics observed in:

- the devices' S-parameters from 50 MHz to 50 GHz in the microwave regime;
- the time-domain large-signal transient drain current observed in pulsed-*IV* measurements.

This paper offers the possibility to include different frequency dispersion effects in a universal, efficient large-signal simulation model. In contrast to most other approaches, the transition between different dispersion states is accurately modeled, offering true broadband description of dispersive devices. The dispersion part is incorporated in a full HFET equivalent circuit containing nonlinear gate current and capacitance characteristics. Being fully implemented into a circuit simulation environment,

the model is then employed in the design and realization of a GaAs pHEMT distributed monolithic microwave integrated circuit (MMIC). The comparison of measured and simulated circuit performance further validates the model.

II. Dispersion Model

A. Single Dispersion Source Approach

The basis of the dispersion model topology discussed here is the assumption that individual dispersion effects introduce an exponentially decaying time-domain characteristic to the free carrier density n_s and, due to the proportionality between carrier density and current, to the resulting drain-source current $I_{\rm ds}$. Applying a step change in either one of the controlling voltages $V_{\rm gs}$ and $V_{\rm ds}$ at time $t = 0$ will result in a step response of the carrier density and the drain current of the form

$$n_s(t) \sim I_{\rm ds}(t) = I_0 + (I_1 - I_0)e^{-\frac{t}{\tau_1}} \tag{1}$$

where τ_1 is the time constant associated with one particular dispersion effect, I_1 is the current flowing immediately after the voltage change when a particular physical condition responsible for dispersion, e.g., channel temperature, trap occupation etc., is still in the state of condition $t < 0$. I_0 is the drain current under the new voltage conditions when the dispersion effect has adapted to the new voltage regime. The approach of (1) implicitly assumes a constant, i.e., time and voltage independent, time constant τ_1.

The assumption of an exponentially decaying step response due to a single dispersion effect is well founded in the case of thermal dispersion as well as trapping/detrapping effects. The frequency dependence introduced by impact ionization to the small-signal characteristics of InP-based HFETs has been shown to obey the same principle [15].

Introducing the Heaviside function $s(t)$, the step response $a(t)$ of the drain current can be written as

$$a(t) = s(t)\left(I_0 + (I_1 - I_0)e^{-\frac{t}{\tau_1}}\right). \tag{2}$$

Equation (2) has the well-known form of a single-pole or first-order system transfer function. Since drain current is a nonlinear function of two independent controlling voltages $V_{\rm gs}$ and $V_{\rm ds}$, the step response to a change in one of the controlling voltages is found by partial differentiation of (2), yielding $a_{\rm gs}(t) = (\partial a(t)/\partial V_{\rm gs})$ and $a_{\rm ds}(t) = (\partial a(t)/\partial V_{\rm ds})$. Differentiation in time-domain results in the pulse responses $h_{\rm gs}(t) = (\partial a_{\rm gs}(t)/\partial t)$ and $h_{\rm ds}(t) = (\partial a_{\rm ds}(t)/\partial t)$. Making use of the Dirac pulse function $\delta(t)$ and its sifting property, they can be written as

$$h_{\rm gs}(t) = \delta(t)\frac{\partial I_1}{\partial V_{\rm gs}} - \frac{s(t)}{\tau_1}\left(\frac{\partial I_1}{\partial V_{\rm gs}} - \frac{\partial I_0}{\partial V_{\rm gs}}\right)e^{-\frac{t}{\tau_1}} \tag{3}$$

$$h_{\rm ds}(t) = \delta(t)\frac{\partial I_1}{\partial V_{\rm ds}} - \frac{s(t)}{\tau_1}\left(\frac{\partial I_1}{\partial V_{\rm ds}} - \frac{\partial I_0}{\partial V_{\rm ds}}\right)e^{-\frac{t}{\tau_1}}. \tag{4}$$

The proposed equivalent circuit used to obtain the above dispersive drain current characteristics is shown in Fig. 1.

In parallel to the static current source I_0, the dispersion current is formed by a voltage-controlled current source $(1/R_x)V_x$,

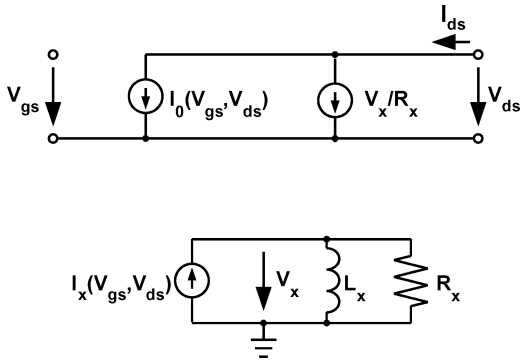

Fig. 1. Large-signal equivalent circuit of a single dispersion effect.

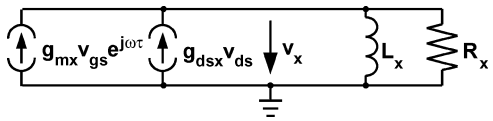

Fig. 2. Linearization of the dispersion model (dispersion source only).

which translates a nonlinear voltage V_x, obtained from a parallel L-R circuit, into current. The total drain current $I_{\rm ds}$ of the proposed topology can be written as

$$I_{\rm ds} = I_0 + \frac{1}{R_x}V_x = I_0 + I_x\frac{j\omega L_x}{R_x + j\omega L_x} \tag{5}$$

where I_0 and I_x are controlled by two voltages: I_0, $I_x = f(V_{\rm gs}, V_{\rm ds})$. The dispersion current source is set to $I_x = I_1 - I_0$. The linearized small-signal representation of the dispersion model is shown in Fig. 2.

Output related Y-parameters of the circuit are found to be

$$\begin{aligned} Y_{21} &= \frac{\partial I_0}{\partial V_{\rm gs}} + \frac{1}{R_x}\frac{\partial V_x}{\partial V_{\rm gs}} \\ &= g_{m0} + g_{mx} - g_{mx}\frac{R_x}{L_x}\cdot\frac{1}{\frac{R_x}{L_x} + j\omega} \end{aligned} \tag{6}$$

$$\begin{aligned} Y_{22} &= \frac{\partial I_0}{\partial V_{\rm ds}} + \frac{1}{R_x}\frac{\partial V_x}{\partial V_{\rm ds}} \\ &= g_{\rm ds0} + g_{\rm dsx} - g_{\rm dsx}\frac{R_x}{L_x}\cdot\frac{1}{\frac{R_x}{L_x} + j\omega} \end{aligned} \tag{7}$$

where g_{mx} and $g_{\rm dsx}$ are the partial derivatives of the current source $I_{\rm dsx}$ against $V_{\rm gs}$ and $V_{\rm ds}$, respectively. Equation (6) neglects the transit time τ, which only has an impact at millimeter-wave frequencies. The parameters g_{m0} (g_{mx}) and $g_{\rm ds0}$ $(g_{\rm dsx})$ are related by the integrability condition [16], since they derive from a common current function $I_0(V_x/R_x)$. The right terms in (6) and (7) can easily be transformed into time domain using Fourier transformation and the Dirac pulse function $\delta(t)$. The resulting pulse responses $h_{Y21}(t)$ and $h_{Y22}(t)$ of the linearized drain current due to a change in controlling voltages are

$$h_{Y21}(t) = \delta(t)(g_{m0}+g_{mx}) - s(t)\left(g_{mx}\frac{R_x}{L_x}\right)e^{-\frac{t}{L_x/R_x}} \tag{8}$$

$$h_{Y22}(t) = \delta(t)(g_{\rm ds0}+g_{\rm dsx}) - s(t)\left(g_{\rm dsx}\frac{R_x}{L_x}\right)e^{-\frac{t}{L_x/R_x}}. \tag{9}$$

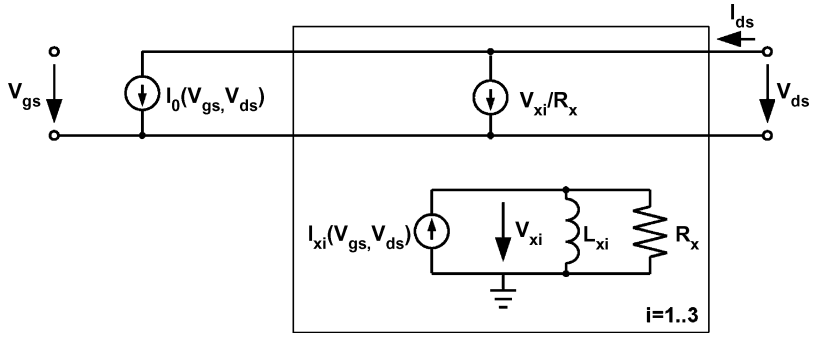

Fig. 3. Incorporation of several dispersion sources within the large-signal model topology.

The equivalent circuit satisfies the initial assumption of a single-pole circuit response, i.e., (8) and (9) equal (3) and (4) for $(\partial I_1/\partial V_{\rm gs}) = g_{m0} + g_{mx}$, $(\partial I_0/\partial V_{\rm gs}) = g_{m0}$, $(\partial I_1/\partial V_{\rm ds}) = g_{\rm ds0} + g_{\rm dsx}$, $(\partial I_0/\partial V_{\rm ds}) = g_{\rm ds0}$, and $\tau_1 = (1/\omega_1) = (L_x/R_x)$, where $\omega_1 = 2\pi f_1$ can be defined as the corner frequency of the dispersion effect. The dispersion time constant can therefore be controlled by an appropriate choice of L_x/R_x.

B. Multiple Dispersion Sources

Individual dispersion effects with different time constants can now be incorporated in the model by using several dynamic sources in parallel (Fig. 3).

The total drain current now is

$$I_{\rm ds} = I_0 + \sum_{i=1\ldots n} I_{xi} \frac{j\omega L_{xi}}{R_x + j\omega L_{xi}} \tag{10}$$

where n is the number of dispersion sources and

$$I_{xi} = I_i - I_{i-1}, i = 1, \ldots, n \tag{11}$$

is the current attributed to dispersion source i. L_{xi}/R_x lead to the respective time constants of dispersion source i.

The parallel placement of several dispersion sources and the current definition of (11) will lead to a total drain current in the frequency domain of I_i for $f_i < f < f_{i+1}$, where $f_i = (1/2\pi)(R_x/L_{xi})$ are the corner frequencies of the individual dispersion sources as deduced above. The dispersion sources are numbered with increasing corner frequency $f_i > f_{i-1}$, that means $L_{xi} > L_{x,i-1}$. Small-signal conductances of the circuit result accordingly.

III. Extraction Procedure

In addition to an accurate drain current model, the complete transistor model will also have to describe reactive effects in the device, e.g., nonlinear gate capacitance. In the case of transistors fabricated with a Schottky contact, nonlinear gate current will be included. The dispersion model therefore is embedded into a full large-signal FET equivalent circuit [17]. Here, we concentrate on the extraction of the dispersive drain current model.

Many different model equations have been developed for description of nonlinear drain current characteristics in HFETs. Among the most popular analytical expressions are the Curtice–Ettenberg [18], Angelov/Chalmers [19], and Tajima [20] models. The dispersion model approach described here is not restricted to a particular current equation. In fact, different expressions could be employed for the nonlinear current characteristics, provided simulation convergence is met for their combination. Here we use a modified COBRA model [21] and extract parameter sets for all drain current characteristics required in the dispersion model. This compact and efficient expression has been proven to be well suited to describe drain current nonlinearities in HFETs [17] as well as in RF metal–oxide–semiconductor FETs [22], [23].

The static model is derived from dc drain current measurements. In terms of dispersion, the drain current under all control voltage conditions reaches the value where all dynamic current contributions have disappeared: channel temperature adjusts to static power, trap occupation settles at an equilibrium between caption and re-emission, interface states reach an equilibrium occupation, and impact ionization can build up for high enough field strengths. In the model, all dispersion voltages V_x become zero. Depending on the technology and its effective thermal conduction, static characteristics experience self-heating to a more or less pronounced extend. In the GaAs pHEMT under static and very low frequency conditions, the approach taken in [24] is adopted.

A. Dynamic IV From Pulsed-IV Measurements

Originating from a quiescent point $Q = (V_{\rm gs0}, V_{\rm ds0})$, short pulses to a voltage condition $A = (V_{\rm gs}, V_{\rm ds})$ with pulse length $t_{\rm pulse}$ and period $t_{\rm cycle}$ are applied to the device for measuring the current at A. Thus, when sweeping A over the whole *IV* plane and providing a large enough $t_{\rm cycle}$ for the device to regain its static condition after each pulse, one obtains dynamic *IV* characteristics, which will be a function of the pulse width and the quiescent condition $I_{\rm ds,ac} = f(t_{\rm pulse}, Q)$.

Dispersion effects with time constants larger than the pulse width will not adapt rapidly enough to the new voltage conditions and are therefore eliminated from the resulting *IV* characteristics. The measurement system used here is an Accent Diva D225 pulsed *IV* analyzer, capable of delivering pulses as short as $t_{\rm pulse} \geq 0.1$ μs to the device. Plotting the drain current in a certain voltage point A versus pulse width yields the transient pulse response of the device (see Fig. 7). One observes a current response corresponding to two exponentially decaying functions with time constants $\tau_1 = 1$ μs and $\tau_2 = 200$ μs. The function used to describe this behavior is

$$I_{\rm ds}(t) = I_0 + (I_1 - I_0)e^{-\frac{t}{\tau_1}} + (I_2 - I_1)e^{-\frac{t}{\tau_2}}. \tag{12}$$

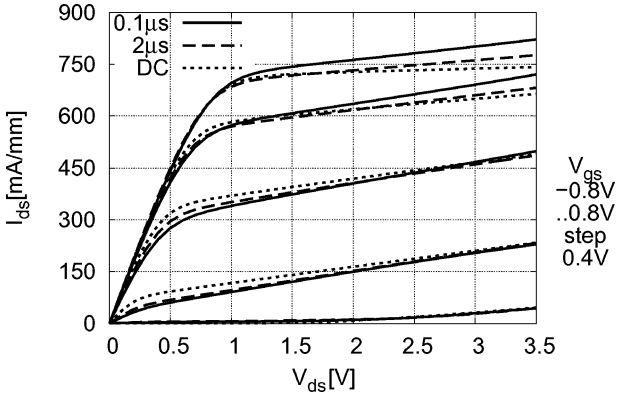

Fig. 4. Modeled dynamic *IV* characteristics of a 2×20 μm GaAs pHEMT based on pulsed measurements with different pulse widths.

Applying this function over the whole *IV* plane results in two nonlinear dynamic current sources I_1 and I_2. Trapping and detrapping effects are mainly associated with the short time constant dispersion, whereas the large time constant effect is usually associated with thermal dispersion. Since the two time constants are separated by about two orders of magnitude, it is also possible for I_1 to be attributed to the pulsed *IV* characteristic obtained with medium pulse widths, where the dispersion effect(s) responsible for the fast change in current have adapted and allowed the current to settle at the intermediate value before the final change due to the dispersion effect with a larger time constant. In the case of the GaAs pHEMT, this is true for pulse widths of $t_{\rm pulse} \approx 2$ μs

$$I_1 \approx I_{\rm ds,ac}|_{t_{\rm pulse}=2\ \mu{\rm s},hot}. \tag{13}$$

The second dispersion source describes the current characteristics obtained with minimum pulse widths

$$I_2 \approx I_{\rm ds,ac}|_{t_{\rm pulse}=0.1\ \mu{\rm s},hot}. \tag{14}$$

The model is extracted from and will be valid under a "hot," i.e., conducting and saturated, quiescent condition, corresponding to a class A operation of the device. The resulting *IV* characteristics for I_1 and I_2 of a 2×20 μm GaAs device are shown in Fig. 4 together with the static curves.

The dependence of pulsed-*IV* characteristics on the choice of the quiescent point constitutes a limitation to the validity of the model, in the same manner as a conventional nondispersive model based purely on pulsed-*IV* data. Dedicated models have to be extracted for the simulation of e.g., startup transients and pulsed amplifiers.

B. Dynamic IV From Trans- and Output Conductance

The use of pulsed *IV* measurements allows for the exclusion of dispersion effects with time constants larger than the minimum pulse length. Some dispersion effects, however, like impact ionization current, show time constants orders of magnitude smaller, with corresponding cutoff frequencies lying in the upper megahertz range.

Another method for obtaining dynamic *IV* characteristics is the use of small-signal transconductance $g_{m,ac}$ and output

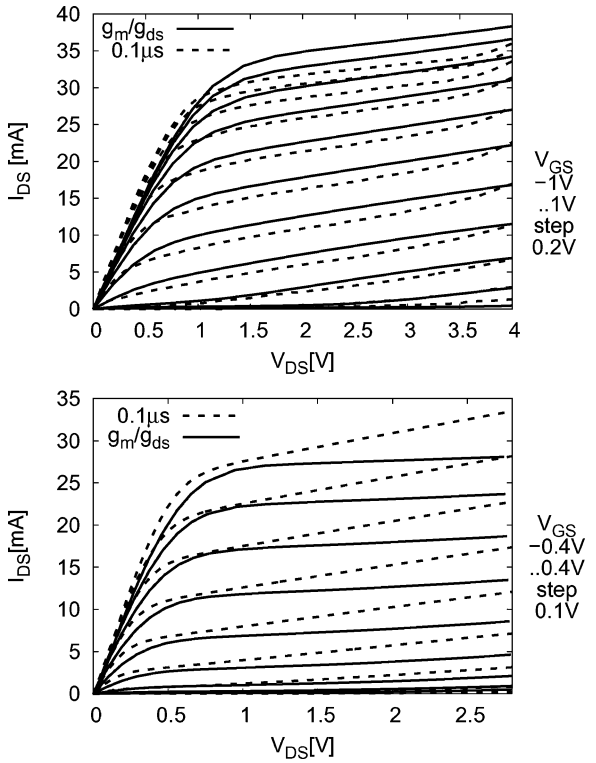

Fig. 5. Dynamic *IV* obtained from numerical integration of multibias transconductance and output conductance information for frequencies beyond 5 GHz. (Top) GaAs pHEMT. (Bottom) InP pHEMT. Comparison to pulsed-*IV* with 0.1 μs pulse width (dotted lines).

conductance $g_{\rm ds,ac}$, obtained from multibias S-parameter measurements at microwave frequencies [25], [26]. Many excellent models have been built using table-based splines [27]. Since, even at microwave frequencies, g_m and $g_{\rm ds}$ should result from linearization of a nonlinear drain-source current in the transistor, it makes sense to represent this current by the same analytical expression used for modeling static and pulsed-*I–V* characteristics, i.e., the COBRA model. One therefore uses numerical integration of the small-signal information to obtain dynamic *IV*

$$I_{\rm ds,ac} = I_{\rm ds0} + \int_C g_{m,ac}\partial V_{\rm gs} + g_{\rm ds,ac}\partial V_{\rm ds}. \tag{15}$$

Since $g_{m,ac}$ and $g_{\rm ds,ac}$ have been obtained independently from individual small-signal measurements, a path dependence of the numerical integration and with it a quantifiable error to the resulting dynamic *IV* behavior is introduced. The integration path C and quiescent current $I_{\rm ds0}$ at point $Q = (V_{\rm gs0}, V_{\rm ds0})$ for integration are chosen in order to minimize the global relative deviation between the measured $g_{m,ac}$ and $g_{\rm ds,ac}$ and the partial derivatives of the dynamic current. In practice, the integration error increases towards the boundaries, notably in the linear and subthreshold operating regimes. Global validity is therefore limited. This method leads to the *IV* characteristics shown in Fig. 5.

For the InP device, the optimum quiescent point for integration was below threshold and at $V_{\rm ds0} = 1.6$ V. The integration path used alternating steps in $V_{\rm ds}$ and $V_{\rm gs}$ direction on the measured voltage grid. For the GaAs device, integration originated

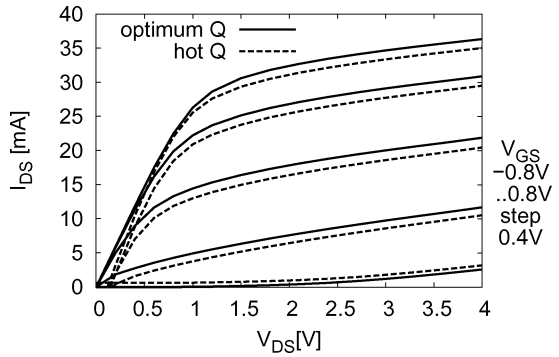

Fig. 6. "Hot" quiescent condition for numerical integration introduces essentially a shift in threshold voltage to the *IV* characteristics, shown here for the GaAs device.

at subthreshold and $V_{\rm ds0} = 0$ V with alternating steps on the voltage grid. Fig. 6 shows the *IV* characteristics obtained for the GaAs device when integration originates in a "hot" quiescent condition with an integration path which first follows constant $V_{\rm ds}$, then constant $V_{\rm gs}$ on the measured voltage grid. The result is essentially a shift of the threshold voltage.

In both the GaAs and the InP device, a significant difference between the dynamic *IV* obtained from pulsed measurements with minimum pulse width and those obtained from numerical integration is observed. In the GaAs pHEMT, the main effect can clearly be linked to the onset of impact ionization at high drain potentials, which has disappeared in the numerically integrated characteristics. The InP device also shows reduced output conductance in the numerically integrated characteristics. However, here the physical effect responsible might be impact ionization or the formation of parasitic channels. Being of empirical nature, the presented modeling method allows for physical interpretation only in the sense of interpreting the impact of dispersion effects with different time constants on drain current characteristics, e.g., the reduction of output conductance. The physical nature of individual dispersion effects is not considered.

IV. Model Verification

Model implementation is straightforward, since the equivalent circuit consists of purely electrical elements, mainly voltage-controlled current sources. At present, the model is fully implemented into the Agilent ADS design environment and can be used for small- and large-signal simulations in the frequency and time domain. As mentioned before, the full model contains all typical HFET elements, mainly the nonlinear gate-source and gate-drain capacitance and gate diodes. In terms of dispersion, three dispersion circuit branches $I_{1,...,3}$ are included.

A. Time Domain

First, the model is used in a transient analysis to simulate the step response of the drain current. The result is shown together with measured values in Fig. 7 for the GaAs-based device. As derived in the modeling approach, the model answers with exponentially decaying current characteristics in the time domain, of which two are visible on the microsecond time scale. Comparison to the measured values shows excellent agreement. In qualitative

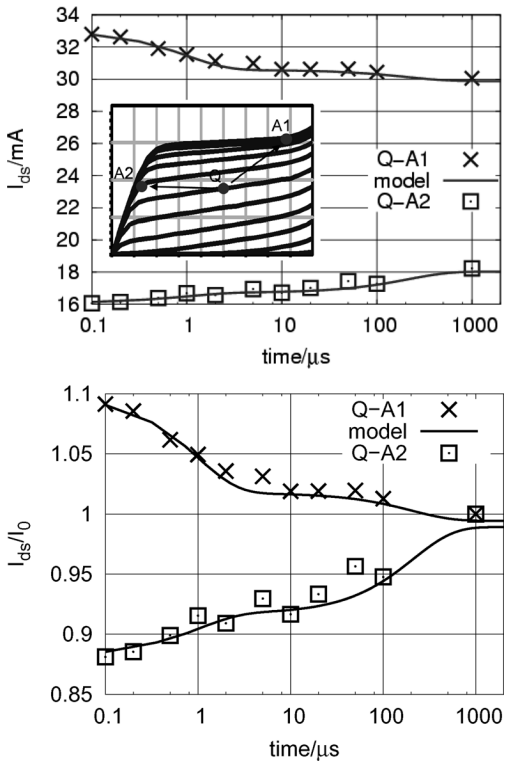

Fig. 7. Transient step response of drain current when stepping from $Q = (0\ \mathrm{V}, 2\ \mathrm{V})$ to $A1 = (0.8\ \mathrm{V}, 3.5\ \mathrm{V})$ and $A2 = (0.2\ \mathrm{V}, 0.6\ \mathrm{V})$. Measurement (dots) and modeled values (lines).

terms, this confirms the modeling approach and the assumption of exponential dispersion characteristics. In quantitative terms, the agreement between measurement and model confirms the suitability of the employed nonlinear current expression.

B. Frequency Domain

The model is also used for simulating S-parameters and comparing them to measurements. For both the GaAs- and the InP-based device, bias conditions are chosen where the impact of frequency dispersion is important. Dispersion effects show up noticeably in S_{21} and S_{22}. Fig. 8 shows the GaAs pHEMT biased in $Q = (0.2\ \mathrm{V}, 3.9\ \mathrm{V})$. Fig. 9 is for the InP device biased in a more typical point $Q = (0.1\ \mathrm{V}, 2.8\ \mathrm{V})$, which corresponds to maximum gain $(g_{m,\max})$ in this technology. In its implemented form, the model allows one to disable the dispersion part and to attribute purely static or purely dynamic characteristics to the remaining (nondispersive) current source $I_{\rm ds} = I_0$. These nondispersive characteristics are also included in the graphs. The comparison of simulated and measured data therefore both validates the model and allows one to investigate the influence of dispersion on the device and circuit level (see Section V).

The S-parameter characteristics, when translated into Y-parameters, correspond to the frequency response derived in (6) and (7), confirming the exponential nature even of those dispersion effects with very small time constants. The qualitative difference stems from the fact that a linearized large-signal model will never be as accurate as the corresponding small-signal model in a particular bias point. In fact, using the small-signal model, one can perfectly match the model to the measured S-parameters. The time constant/corner frequency of the third

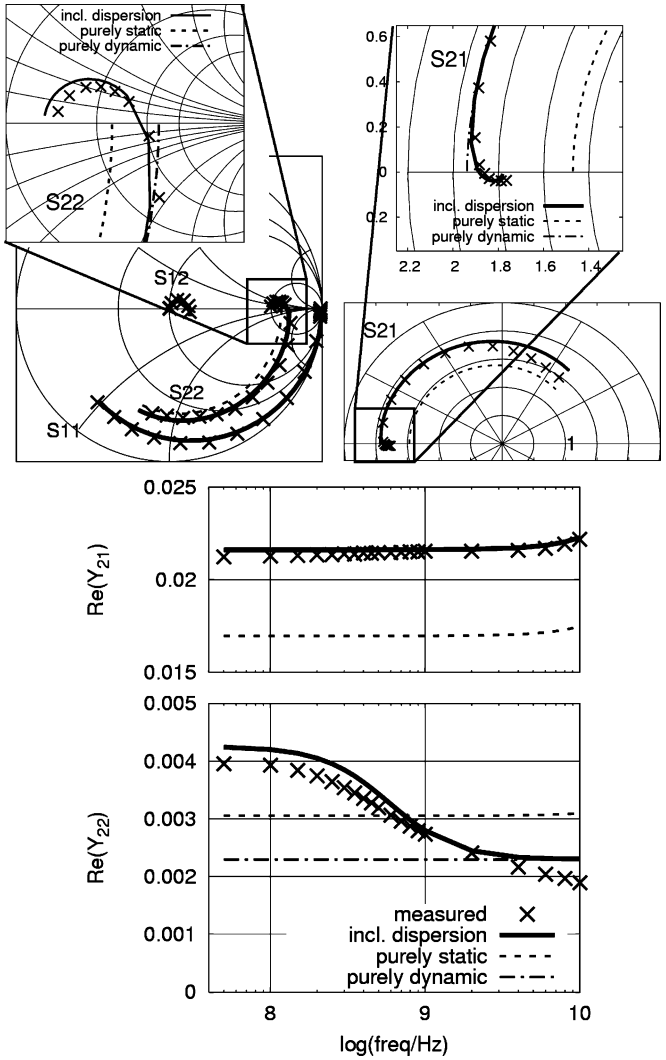

Fig. 8. Measured and modeled S-parameters (50 MHz–50 GHz) of the GaAs pHEMT under bias conditions $Q = (0.2\ \mathrm{V}, 3.9\ \mathrm{V})$. Effects of dispersion on S_{21} and S_{22} are enlarged and compared to models based on purely static and purely dynamic drain current characteristics. (Bottom) Real parts of output related Y-parameters in the lower frequency range.

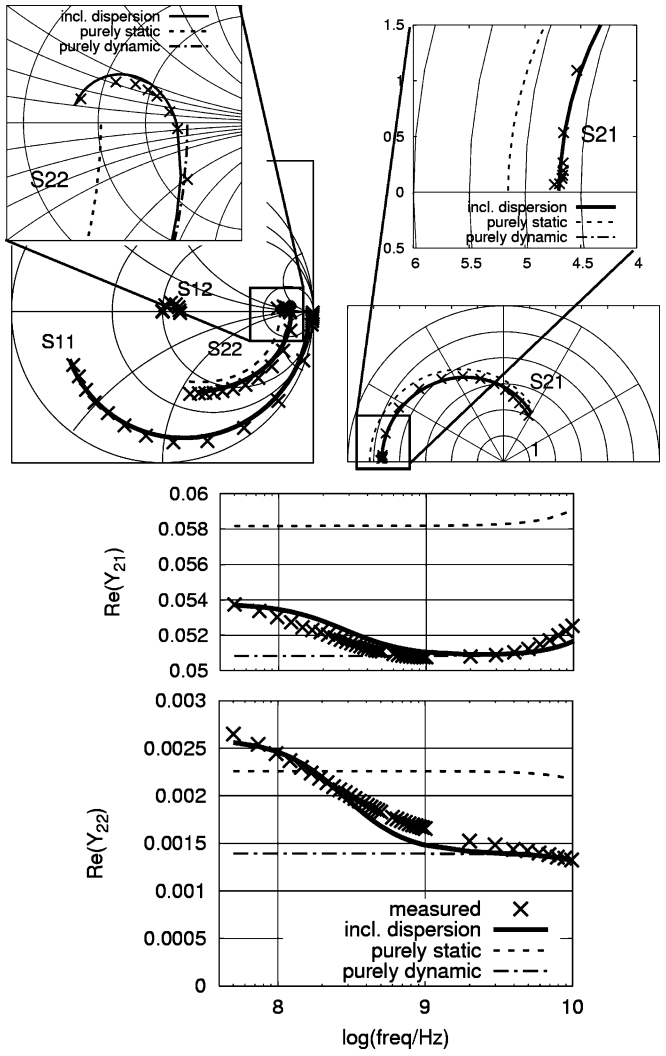

Fig. 9. S-parameters (50 MHz–50 GHz) of the InP pHEMT under bias conditions $Q = (0.1\ \mathrm{V}, 2.8\ \mathrm{V})$ in a comparison to models based on dispersive as well as purely static and purely dynamic drain current characteristics. (Bottom) Real parts of output related Y-parameters in the lower frequency range.

dispersion source which describes the microwave frequency *IV* characteristics is derived from the S-parameters and found to be

$$f_{3,\mathrm{GaAs}} = (2\pi\tau_{3,\mathrm{GaAs}})^{-1} = 560\ \mathrm{MHz} \quad (16)$$

$$f_{3,\mathrm{InP}} = (2\pi\tau_{3,\mathrm{InP}})^{-1} = 270\ \mathrm{MHz}. \quad (17)$$

At moderate frequencies, trans- and output conductance are derived from the real parts of Y_{21} and Y_{22}, respectively. These data, together with the comparison to the full dispersion model and nondispersive models, are shown in Figs. 8 and 9 for both devices. Below f_3, the nondispersive dynamic model deviates in output conductance by up to -42% for the GaAs device and -48% for the InP device, while transconductance is not significantly altered by this high-frequency dispersion effect.

V. Validation in MMIC Performance

Based on the model, a traveling-wave MMIC has been designed and fabricated [28] using a power variant of the GaAs pHEMT technology whose active devices have an f_T of 75 GHz. The MMIC has dual functionality: it can serve as ultrabroadband mixer or variable gain amplifier (VGA). The analysis of both operation types requires a nonlinear model. The dispersion part of the model uses two dynamic sources reflecting multiple pulse-width *IV* characteristics of the transistors, in addition to the static one. This ensures maximum global validity, since dynamic *IV* from numerical integration contains inaccuracies in the linear and subthreshold regimes, as explained in Section III-B.

A. MMIC Design and Realization

Cascode amplifier cells with variable current-voltage feedback, realized by an FET biased in its linear operating region, are used in an eight-stage distributed circuit configuration (Fig. 10). Input and output of the cascodes as well as the feedback transistor gate are embedded into inductive microstrip lines, forming artificial 50-Ω transmission lines and leading to the well-known bandwidth enhancement of traveling-wave circuits.

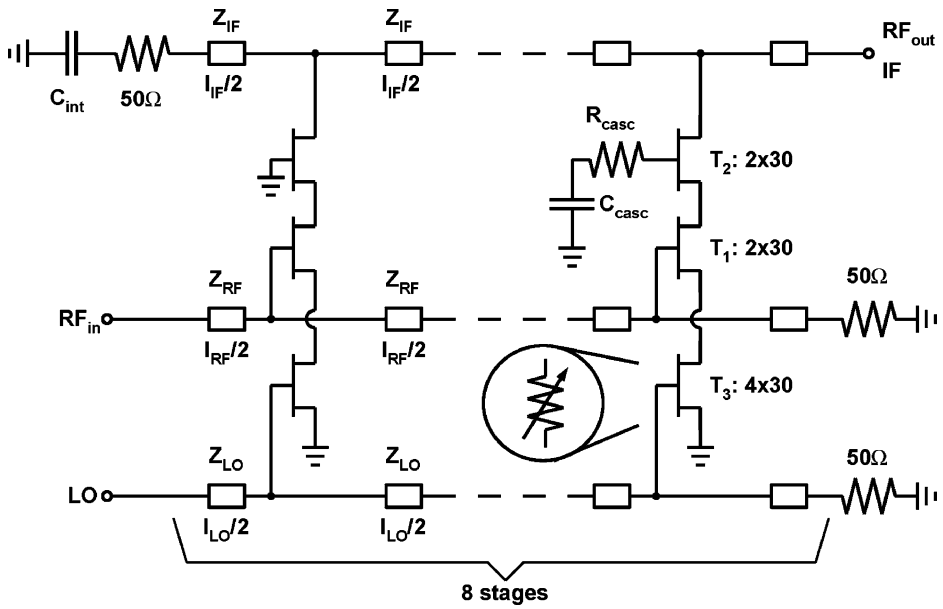

Fig. 10. Distributed circuit topology for mixer and VGA operation. Eight cascode stages with resistive source feedback are embedded into inductive transmission lines.

By applying a local oscillator drive to the feedback line the device may be operated as a mixer, exhibiting measured conversion loss of 2 dB in a bandwidth exceeding 50 GHz. Variable gain amplification is obtained by applying a controlling bias to the feedback line. The gain can be controlled between 5–12 dB with a near-constant bandwidth of up to 43 GHz. The current–voltage feedback topology is particularly challenging for the model quality in terms of frequency dispersion. It uses a scaled transistor (T3) biased in its linear operating region to obtain the feedback effect. Here, dispersion effects show significant differences between static and dynamic *IV* characteristics. For small-signal analysis, an accurate prediction of the bias situation is required in order to linearize the device in a region where both its trans- and output conductance are highly nonlinear and dispersive. Under large-signal conditions, e.g., for mixer operation, the feedback FET is driven between linear, knee, and saturated regimes.

B. Circuit Performance

The model has been shown to predict amplifier gain and bandwidth and, more importantly, mixer conversion gain to a high degree of accuracy [29]. It was also shown that the model allows to correctly analyze power-added effiency (PAE) due to its inherent capability of predicting dynamic gain and gain compression together with static power consumption. However, the error introduced to PAE by purely static or purely dynamic *IV* models is not very pronounced, since the MMIC, designed for high-frequency operation, uses small gate width devices whose *IV* characteristics show only a moderate impact of, e.g., self-heating.

However, a significant impact on circuit simulation using nondispersive models is observed in the gain versus control voltage (gate bias of feedback transistor T3) characteristics. Fig. 11 shows small-signal gain versus control voltage at 25 GHz f_{RF}. Bias conditions for maximum gain are $V_{DD} = 6$ V (drain supply), $V_{G,T1} = -0.15$ V (gate voltage of transistor T1), $V_{G,T2} = 3$ V, and $V_{G,T3} = 0$ V. T3 therefore operates

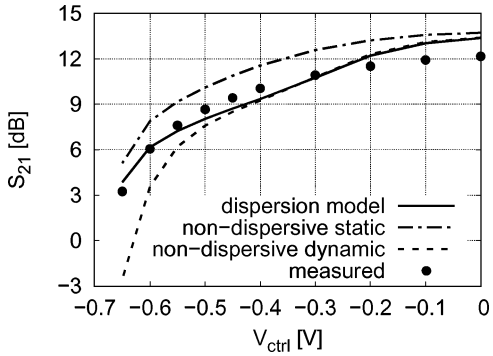

Fig. 11. Amplifier gain versus control voltage at 25 GHz. Only the dispersion model is capable of predicting correct gain in different bias regimes.

in its linear region. The total supply current is 134 mA (model prediction is 131 mA). The purely dynamic model's prediction deviates from measurements when T3 is biased in regions of large differences between static and dynamic characteristics. The static model correctly describes gain reduction but deviates in total gain since it undervalues the feedback effect resulting from the output conductance of T3.

VI. Conclusion

The presented nonlinear frequency dispersion model is developed for the efficient simulation of MMIC systems under broadband linear as well as nonlinear operating conditions. It is universally applicable to dispersive HEMT technologies, enabling the inclusion of individual dispersion effects with different time constants. The model extraction procedure is based on data from standard measurement techniques. The compact dispersion model is integrated into a standard nonlinear FET equivalent circuit. Being fully implemented into a circuit simulation environment, it is found to accurately predict device behavior and full MMIC characteristics from dc up to microwave frequencies, including the transition between individual dispersion states.

ACKNOWLEDGMENT

The authors express their gratitude to Innovative Processing AG and United Monolithic Semiconductors for providing the transistor samples of their HEMT processes as well as for MMIC production.

REFERENCES

[1] J. Conger, A. Peczalski, and M. S. Shur, "Modeling frequency dependence of GaAs MESFET characteristics," *IEEE J. Solid-State Circuits*, vol. 29, no. 1, pp. 71–76, Jan. 1994.

[2] S. Choi and M. B. Das, "Origin and modeling of the frequency dependent output conductance in microwave GaAs MESFET's with buried p layer," *IEEE Trans. Electron Devices*, vol. 41, no. 10, pp. 1725–1733, Oct. 1994.

[3] C. J. Wei, Y. A. Tkachenko, and D. Bartle, "Table-based Dynamic FET model assembled from small-signal models," *IEEE Trans. Microw. Theory Tech.*, vol. 47, no. 6, pp. 700–705, Jun. 1999.

[4] J. W. Lee and K. J. Webb, "A temperature-dependent nonlinear analytic model for AlGaN-GaN HEMTs on SiC," *IEEE Trans. Microw. Theory Tech.*, vol. 52, no. 1, pp. 2–9, Jan. 2004.

[5] J. M. Golio, M. G. Miller, G. N. Maracas, and D. A. Johnson, "Frequency-dependent electrical characteristics of GaAs MESFETs," *IEEE Trans. Electron Devices*, vol. 37, no. 5, pp. 1217–1227, May 1990.

[6] A. Santarelli, G. Zucchelli, R. Paganelli, G. Vannini, and F. Filicori, "Equivalent-voltage description of low-frequency dispersive effects in large-signal FET models," in *Proc. Eur. GaAs Rel. III-V Compounds Applicat. Symp.*, London, Sep. 2001, pp. 45–48.

[7] G. Simin, M. A. Khan, M. S. Shur, and R. Gaska, "Insulated gate III-N heterostructure field-effect transistors," *Int. J. High-Speed Electron. Syst.*, vol. 14, no. 1, pp. 197–224, 2004.

[8] S. S. Islam and A. F. M. Anwar, "Self-heating and trapping effects on the RF performance of GaN MESFETs," *IEEE Trans. Microw. Theory Tech.*, vol. 52, no. 4, pp. 1229–1236, Apr. 2004.

[9] M. Schroter, HICUM: A scalable physics-based compact bipolar transistor model—Description of model version 2.1 Dec. 2000 [Online]. Available: www.iee.et.tu-dresden.de

[10] V. Rizzoli, D. Masotti, and F. Mastri, "Behavioural modelling of thermally induced distortion in RF/microwave nonlinear subsystems," in *Proc. 34th Eur. Microw. Conf.*, Amsterdam, The Netherlands, Sep. 2004, pp. 845–848.

[11] H. Ku and J. S. Kenney, "Behavioral modeling of nonlinear RF power amplifiers considering memory effects," *IEEE Trans. Microw. Theory Tech.*, vol. 51, no. 12, pp. 2495–2504, Dec. 2003.

[12] "United Monolithic Semiconductors," [Online]. Available: www.ums-gaas.com

[13] D. Keiper, P. Velling, A. Brennemann, M. Agethen, C. van den Berg, and R. M. Bertenburg, "MOVPE growth of InAlAs using TBAs and DitBuSi for HEMT applications," *J. Cryst. Growth*, vol. 248, pp. 153–157, Feb. 2003.

[14] I. Kallfass, T. J. Brazil, B. OhAnnaidh, P. Abele, T. Hackbarth, M. Zeuner, U. König, and H. Schumacher, "Large signal modelling including low-frequency dispersion of N-channel SiGe MODFETs and MMIC applications," *Solid-State Electron.*, vol. 48, no. 8, pp. 1433–1441, Aug. 2004.

[15] R. Reuter, M. Agethen, U. Auer, S. van Waasen, D. Peters, W. Brockerhoff, and F. J. Tegude, "Investigation and modeling of impact ionization with regard to the RF and noise behaviour of HFET," *IEEE Trans. Microw. Theory Tech.*, vol. 45, no. 6, pp. 977–983, Jun. 1997.

[16] A. D. Snider and P. Wilson, "A generalized Dirichlet principle for smoothing small-signal measurements," *IEEE Trans. Microw. Theory Tech.*, vol. 47, no. 5, pp. 636–639, May 1999.

[17] I. Kallfass, C. Schick, H. Schumacher, and T. J. Brazil, "A universal large-signal model for hetero field-effect transistors," in *Proc. 12th GaAs Symp. Eur. Microw. Week*, Amsterdam, The Netherlands, Oct. 2004, pp. 55–58.

[18] W. R. Curtice and M. Ettenberg, "A nonlinear GaAsFET model for use in the design of output circuits for power amplifiers," *IEEE Trans. Microw. Theory Tech.*, vol. MTT-33, no. 12, pp. 1383–1394, Dec. 1985.

[19] I. Angelov, H. Zirath, and N. Rorsman, "A new empirical nonlinear model for HEMT and MESFET devices," *IEEE Trans. Microw. Theory Tech.*, vol. 40, no. 12, pp. 2258–2266, Dec. 1992.

[20] Y. Tajima and P. D. Miller, "Design of broadband power GaAs FET amplifiers," *IEEE Trans. Microw. Theory Tech.*, vol. MTT-32, no. 3, pp. 261–267, Mar. 1984.

[21] V. I. Cojocaru and T. J. Brazil, "A scalable general-purpose model for microwave FET's including DC/AC dispersion effects," *IEEE Trans. Microw. Theory Tech.*, vol. 45, no. 12, pp. 2248–2255, Dec. 1997.

[22] B. OhAnnaidh and T. J. Brazil, "A globally-continuous, charge-conservative, nonlinear equivalent circuit model for RF MOSFETs," in *Proc. 11th GaAs Symp. Eur. Microw. Week*, Munich, Germany, Sep. 2003, pp. 65–68.

[23] T. J. Brazil, I. Kallfass, B. OhAnnaidh, and M. Wren, "Nonlinear device modelling of Si CMOS, SiGe HFET and GaAs pHEMT," in *IEEE MTT-S Int. Microw. Symp. Workshop*, Fort Worth, Jun. 2004.

[24] P. C. Canfield, S. C. F. Lam, and D. J. Allstot, "Modelling of frequency and temperature effects in GaAs MESFETs," *IEEE J. Solid-State Circuits*, vol. 25, no. 2, pp. 299–306, Feb. 1990, CD ROM.

[25] M. Berroth and R. Bosch, "High-frequency equivalent circuit of GaAs FET's for large-signal applications," *IEEE Trans. Microw. Theory Tech.*, vol. 39, no. 2, pp. 224–229, Feb. 1991.

[26] G. Dambrine, A. Cappy, F. Heliodore, and E. Playez, "A new method for determining the FET small-signal equivalent circuit," *IEEE Trans. Microw. Theory Tech.*, vol. 36, no. 7, pp. 1151–1159, Jul. 1988.

[27] K. Koh, H. M. Park, and S. Hong, "A spline large-signal FET model based on bias-dependent pulsed I-V measurement," *IEEE Trans. Microw. Theory Tech.*, vol. 50, no. 11, pp. 2598–2603, Nov. 2002.

[28] I. Kallfass, H. Schumacher, T. Purtova, A. Brokmeier, and W. Ludwig, "One single travelling-wave MMIC for highly linear broadband mixers and variable gain amplifiers," in *IEEE MTT-S Int. Microw. Symp.*, Long Beach, CA, Jun. 2005, CD ROM.

[29] I. Kallfass, C. Zhang, J. Grünenpütt, C. Teyssandier, and H. Schumacher, "Verification of a frequency dispersion model in the performance of a GaAs pHEMT travelling-wave MMIC," in *Proc. Eur. Gallium Arsenide Other Compound Semiconductors Applicat. Symp.*, Paris, Oct. 2005, pp. 381–384.

Ingmar Kallfass was born in Stuttgart, Germany, on September 9, 1973. He received the Dipl.-Ing. degree in electrical engineering from Stuttgart University, Stuttgart, Germany, in 2000.

In 2001, he was with the National University of Ireland, Dublin, in the framework of the European Commission's Training and Mobility of Researchers Programme, with a focus on nonlinear modeling of SiGe HFET devices. In 2002, he joined the Department of Electron Devices and Circuits, University of Ulm, Ulm, Germany, as a Research and Teaching Assistant. Since 2006, he has been with the Fraunhofer Institute for Applied Solid-State Physics, Freiburg, Germany. His research interests are in the field of millimeter-wave circuit design as well as transistor modeling.

Hermann Schumacher (M'93) was born in Siegen, Germany, on May 5, 1957. He received the Dipl.-Ing. and Doktor-Ing. degrees from Aachen University of Technology (RWTH Aachen), Aachen, Germany, in 1982 and 1986, respectively.

In 1986, he joined Bell Communications Research (Bellcore), Red Bank, NJ, as a Member of Technical Staff, working on InP-based optoelectronic and electronic devices and on wide-band circuit design. In 1990, he joined the University of Ulm, Ulm, Germany, as a Professor in the Department of Electron Devices and Circuits. In 2001, he founded the Competence Center for Integrated Circuits in Communications, a public/private partnership dedicated to research and development in RF and wideband optoelectronic integrated circuits. There, he and his group work predominantly on heterojunction bipolar transistors in the Si/SiGe and AlGaAs/GaAs material systems and their applications in high-speed (mainly wireless) circuits, on improved passive circuit elements on silicon, and on frequency- and time-domain characterization techniques. He is also Director of the International Master Program on Communications Technology, University of Ulm. From 2001 to 2003, he was Vice President for Research with the University of Ulm and is currently heading a committee on internationalization there. He was a Visiting Professor at the University of Wales, Cardiff, U.K., in summer 1991 and Oregon State University, Corvallis, in 1997. In 1996, he spent three months with Bellcore, Red Bank, NJ, as a Consultant on InP HBT technology. He is an author or coauthor of more than 150 publications and conference contributions.

Thomas J. Brazil (F'04) was born in County Offaly, Ireland. He received the B.E. degree in electrical engineering from University College Dublin (UCD), Dublin, Ireland, in 1973 and the Ph.D. degree from the National University of Ireland in 1977.

He subsequently worked on microwave subsystem development at Plessey Research (Caswell), U.K., from 1977 to 1979. After a year as a Lecturer in the Department of Electronic Engineering, University of Birmingham, U.K., he returned to UCD in 1980, where he is now a Professor in the Department of Electronic and Electrical Engineering, holds the Chair of Electronic Engineering, and is Head of the department. He has worked in several areas of science policy, both nationally and on behalf of the European Union. Between 1996 and 1998, he was Coordinator of the European EDGE project, which was the major EU Framework *IV* (ESPRIT) project in the area of high-frequency computer-aided design (CAD). His research interests are in the fields of nonlinear modeling and device characterization techniques, with particular emphasis on applications to microwave transistor devices such as GaAs FET, HEMT, BJT, and HBT. He also has interests in convolution-based CAD simulation techniques and microwave subsystem design.

Prof. Brazil is a Fellow of IEI and a Member of Royal Irish Academy. From 1998 to 2001, he was an IEEE Microwave Theory and Techniques Society (MTT-S) Worldwide Distinguished Lecturer in High-Frequency Applied to Wireless Systems. He is currently a member of the IEEE MTT-1 Technical Committee on CAD.